Since January 2020 Elsevier has created a COVID-19 resource centre with free information in English and Mandarin on the novel coronavirus COVID-19. The COVID-19 resource centre is hosted on Elsevier Connect, the company's public news and information website.

Surface & Coatings Technology 399 (2020) 126163

Contents lists available at ScienceDirect

Surface & Coatings Technology

journal homepage: www.elsevier.com/locate/surfcoat

Antibiofilm coatings through atmospheric pressure plasma for 3D printed surgical instruments

Ignacio Muro-Fraguas[a,*], Ana Sainz-García[a], María López[b], Beatriz Rojo-Bezares[b], Rodolfo Múgica-Vidal[a], Elisa Sainz-García[a], Paula Toledano[b], Yolanda Sáenz[b], Ana González-Marcos[a], Fernando Alba-Elías[a]

[a] Department of Mechanical Engineering, University of La Rioja, C/ San José de Calasanz 31, 26004 Logroño, La Rioja, Spain
[b] Molecular Microbiology Area, Center for Biomedical Research of La Rioja (CIBIR), C/Piqueras 98, 26006 Logroño, La Rioja, Spain

ARTICLE INFO

Keywords:
Atmospheric-pressure cold plasma
Plasma-polymerization
3D printing surgical tools
Antibiofilm coatings
Antimicrobial resistant strains
Hydration layer

ABSTRACT

Recently, medical applications for 3D printing are expanding rapidly and are expected to revolutionize health care, specifically, manufacturing surgical guides and protective face mask against coronavirus (COVID-19). These instruments come in contact with the human tissues, being necessary 3D printed materials free of pathogenic microbes or other contaminants. Therefore, they must be sterilized to avoid that bacteria can attach to the surface and produce biofilm. With the aim of avoiding bacterial biofilm formation and minimize the health risks, acrylic acid (AcAc) coatings applied by plasma-polymerization have been deposited on 3D printed polylactic acid (PLA) Petri dishes. Six antimicrobial-resistant clinical and two susceptible control strains of *Pseudomonas aeruginosa* and *Staphylococcus aureus* species were analyzed. AcAc coatings provide the surface with greater hydrophilicity and, consequently, the formation of a hydration layer, whose thickness is related to the surface roughness. This hydration layer could explain the reduction of bacterial attachment and, consequently, the biofilm formation. Antibiofilm coatings are more successful against *P. aeruginosa* strains than against *S. aureus* ones; due to some coatings presents a smaller topography scale than the *P. aeruginosa* length, reducting the contact area between the bacteria and the coating, and causing a potential rupture of the cellular membrane. AcAc coatings with less number of plasma passes were more effective, and showed up to a 50% relative biofilm reduction (in six of the eight strains studied) compared with the untreated plates.

1. Introduction

The 3D printing technology based on biocompatible printable materials, is capable of manufacturing devices with a complex, specific and accurate geometry for each patient and their anatomy [1]. For these reasons, medical applications for 3D printing technology are expanding quickly [2,3]. In 2006, the 3D printing industry generated $700 million, with only $11 million (1.6%) invested in medical applications. However, in the next decades, 3D printing is expected to achieve $9 billion, spending a quarter of the total on medical applications [4]. The most common medical applications of 3D printing devices are: preoperatory planification, education, clinical training and surgical use (implants, prosthesis and protection devices) [5]. In the past few months, the global coronavirus pandemic (COVID-19) have caused a shortage of personal protective equipment (PPE) worldwide. In order to avoid the lack of protective medical equipment and prevent the spread of COVID-19, 3D printing makers community have started manufacturing specific facial mask and respirators for intensive care unit (ICU) patients. Due to the risks associated with 3D printing medical devices (detailed below) and with the aim of combating COVID-19 disease effectively, the European Commission (DG GROW) has written a list of the 3D printing resources available in Europe [6].

Different materials are used for medical applications according to the employed 3D printing technology: polymers (acrylonitrile butadiene styrene-ABS-, polylactic acid-PLA- and nylon), metals (titanium) or ceramic materials (hydroxyapatite-HA-) [5]. PLA is the most widely used polymer in Fused Filament Fabrication (FFF) technology. PLA is a recyclable, biodegradable and biocompatible thermoplastic; and it is obtained from corn and sugar cane. The low thermal expansion coefficient of PLA facilitates its printing. Therefore, PLA printed parts show

* Corresponding author.
E-mail addresses: ignacio.muro@unirioja.es (I. Muro-Fraguas), ana.sainz@unirioja.es (A. Sainz-García), mlopezm@riojasalud.es (M. López), brojo@riojasalud.es (B. Rojo-Bezares), rodolfo.mugica@unirioja.es (R. Múgica-Vidal), elisa.sainzg@unirioja.es (E. Sainz-García), ptoledano@riojasalud.es (P. Toledano), ysaenz@riojasalud.es (Y. Sáenz), ana.gonzalez@unirioja.es (A. González-Marcos), fernando.alba@unirioja.es (F. Alba-Elías).

https://doi.org/10.1016/j.surfcoat.2020.126163
Received 26 May 2020; Received in revised form 1 July 2020; Accepted 3 July 2020
Available online 05 July 2020

high precision and surface quality [3]. Additionally, toxicity levels associated with PLA filaments during 3D printing are lower than those derived from fossil fuels, like (ABS) [7].

Nevertheless, there are two critical parameters when surgical devices are manufacturing by 3D printing: the porosity and the surface roughness. Surgical instruments require a smooth surface to avoid that it can damage tissues or wear away the tool over time, to limit the risk of bacterial contamination and to guarantee a high corrosion resistance. Nowadays, the use of 3D printing technology is limited in the surgical field because this technology produces rough tools, so after the initial manufacturing process it is necessary to apply additional processes such as electro-chemical machining (ECM), thermal deburring or electro-polishing, for improving the initial surface finish. These processes are critical for 3D printing devices; compromising its mechanical properties [8,9].

Besides, the grooves produced on the tool surface by FFF technology favor the adhesion and proliferation of different microorganisms [10]; requiring sterilization procedures [11]. Attachment is the most crucial stage, because if bacteria adhere successfully to a surface, they will begin to proliferate. Bacterial proliferation is often accompanied by production of an extracellular matrix, leading to biofilm formation [12]. Biofilm production facilitates bacteria survival, protecting them from hostile environments. For this reason, bacterial biofilm formation is one of the main concerns in industrial cleanliness and hospital environment [13].

PLA printed tools are not suitable for autoclave sterilization process, due to the low fusion temperature of PLA (50–60 °C) [11,14]. Therefore, special sterilization protocols are required for the medical applications, such as ethylene oxide [15,16]. It has been demonstrated that sterilization with ethylene oxide is suitable for PLA printed devices without affecting the geometry, chemical and mechanical properties of the printed pieces [7]. However, some researches have described a lot of ethylene oxide sterilization inconveniences. The compound is flammable and toxic, increasing the risk of spontaneous miscarriage; as well as potentially causing cancer, neurological and cognitive impairment, central nervous system depression, skin irritation and gastrointestinal problems. In addition to the problems associated with its toxicity, ethylene oxide sterilization has other disadvantages such as high costs and long processing times [11].

Coatings applied by cold atmospheric pressure plasma technology have been very different industrial sectors: automotive [17], metallurgy [18], renewable energies [19,20], textile [21], biomedical [22] … In the last decade there has been a significant interest in the deposition of functional coatings that will be capable of tuning the physical, chemical and morphological properties of a surface without altering the bulk material. Unlike more traditional methods, the application of coatings by atmospheric pressure plasma polymerization does not require working under vacuum conditions or using solvents; so it is cheap, versatile, clean and the properties of the coatings could be modified by controlling different processing parameters (e.g., passes, power, speed, etc.). Besides, cold plasma treatments are suitable for PLA filaments because the low temperature that is reached during these treatments does not cause damage to heat sensible biomaterials [23]. Many researches have applied atmospheric plasma coatings to reduce bacterial attachment. Stallard et al. [24] quantified the protein adsorption and bacterial adhesion onto silicon and titanium substrates previously modified by atmospheric pressure plasma polymerized siloxane coatings. Fluorinated siloxane coatings increased the hydrophobic wetting behavior and produced a significant reduction of *Staphylococcus aureus* attachment and protein adsorption. Hernández-Orta et al. [25] evaluated the bactericidal capacity of atmospheric pressure plasma polymerized 4-vinyl pyridine (4VP) coatings on high-density polyethylene substrates. The 4VP coatings achieved a complete *E. coli* inactivation. Further explanation of these studies is carried out in a previous work [26], in which we reviewed different mechanisms that employ atmospheric pressure plasma technologies for the deposition of antibiofilm coatings. Among these antibiofilm approaches, coatings that modify the physicochemical surface properties stand out. In food industry, the modification of physicochemical substrate properties can be a good prospect compared with the disadvantages that may arise with other alternatives, such as coatings containing antibacterial and biocidal agents. The coatings that produce a change in the surface properties can decrease biofilm formation avoiding the bacterial adhesion rather than killing them once attached. Besides, this approach does not use biocidal agents, so it gives places to non-toxic surfaces with antibiofilm capacity; which is ideal for food contact surfaces. Functional groups added in the substrate by the fragmentation of the precursor molecules, form a layer of water that generates a steric repulsion and prevent direct contact between bacteria and substrates. However, antibiofilm mechanism is not yet totally understood. In a recent work [27], we applied acrylic acid (AcAc) and tetraethyl orthosilicate (TEOS) plasma-polymerization coatings over 3D printed polylactic-acid (PLA) Petri dishes with the aim of reducing *P. aeruginosa*, *Escherichia coli* and *Listeria monocytogenes* biofilms, three important species in the food industry. AcAc coatings incremented the amount of oxygen functional groups and PLA wettability; and therefore, reduced biofilm formation. PLA substrates coated with one pass of AcAc generated a biofilm production of 47.7% for *L. monocytogenes*, 50.4% for *P. aeruginosa* and 64.1% for *E. coli*; compared to biofilm production on untreated PLA plates.

P. aeruginosa and *S. aureus* are two of the most significant opportunistic pathogens in the clinical field and are capable of causing a broad range of infections. *P. aeruginosa* is responsible of important nosocomial infections, can cause infections normally associated with hospital instruments where the bacteria adheres and adapts (including catheters, stethoscopes, drainage implants …) and causes serious infections in patients who have cronical respiratory issues or immunosuppression [28]. *S. aureus* causes a range of recalcitrant device-related infections, such as intravascular catheter infections, prosthetic joint and valve infections, etc. [29]. The aim of this work was to reduce the microbial adhesion and contamination of PLA 3D printed tools by applying antibiofilm plasma-polymerized coatings using an atmospheric-pressure plasma jet (APPJ) system. Over the last years, numerous studies have described the benefits of using 3D printed instruments in surgical operations but have warned about the risks associated with the contamination of 3D printed surfaces. Hsu et al. [30] evaluated the advantages of employing 3D printing surgical splints and templates during maxillofacial surgery. The 3D printed surgical devices increased the accuracy in repositioning the chin segment. Mardini et al. [31] employed 3D printed positioning instruments (manufactured by stereolithography) to guide the location of osteotomies and the fixation of bone segments. It allowed a more precise and rapid reconstruction. Anton de Vez et al. [32] used a 3D printed PLA surgical guide during a rhinoplasty. They observed that 3D printing technology incremented the accuracy; making the intervention easier and faster than the conventional osteotomy. Chuan et al. [33] designed a 3D printed ABS armband coated with a gelatinous substance used to attach the armband to the patient's burnt skin. This research stablished that 3D printing technology is useful for replacing the current bandages, and consequently, for reducing patients' pain and promoting healing. However, they warned that the material for medical applications should be sterilized easily, so we have to choose them carefully. Currently, due to the lack of personal protective equipment (PPP) along the current coronavirus pandemic, Swennen et al. [34] designed reusable components of the 3D face mask manufactured by 3D printing technology. They warned against the infection risks on 3D printed surfaces and encouraged the worldwide researchers to perform virologic testing on 3D printed parts.

The effectivity of the coatings was evaluated by measuring biofilm biomass produced by multidrug-resistant and susceptible *P. aeruginosa* and *S. aureus* strains. The influence of the number of passes (1, 2, 6 and 12) was characterized from a morphological, physico-chemical and microbiological point of view. For these characterizations, atomic force

microscopy (AFM), scanning electron microscopy (SEM), X-ray photoelectron spectroscopy (XPS) and crystal violet (CV) staining assay for biofilm quantification were used.

2. Experimental

2.1. Materials

White PLA RS PRO with 1.75 mm diameter (RS PRO, UK) was the filament used for the printing of PLA Petri dishes. Acrylic acid tech. 90% (AcAc; ($C_3H_4O_2$)) (Alfa-Aesar, USA) was used as precursor liquid for the plasma-polymerized coatings. After plasma treatments, PLA Petri dishes were covered with 35 mm diameter sterilized polystyrene (PS) lids (Thermo-Scientific, USA) to prevent from environmental contamination.

2.2. 3D printing process

The 3D printer used was "Original Prusa i3 MK3" (Prusa3D, Czech Republic). According to manufacturer recommendations [35], the extruder and the print bed temperatures were 215 °C and 60 °C, respectively. A nozzle of 0.4 mm diameter, a layer thickness of 0.2 mm and a fill of 80% were used for printing the PLA Petris dishes. The 3D printed PLA Petri dishes showed the following geometry: 31 mm inside diameter, 35 mm outside diameter and 15 mm height (Fig. 1[a]). These 3D printed dishes were chosen as the most appropiated tools to analyze the in vitro antibiofilm properties of plasma-polymerized coatings.

2.3. Plasma-polymerization process

Once PLA Petri dishes were printed, the different plasma-polymerized coatings (Table I) were applied using an APPJ system PlasmaSpot500® (MPG, Luxemburg). This system consists of an Al_2O_3 dielectric tube between two cylindrical electrodes, one external connected to a high voltage source and the other one internal and grounded (Fig. 1[b–c]).

Table I
Sample identification and number of plasma-polymerized passes.

Samples	Passes
Untreated	–
Ac1p	1
Ac2p	2
Ac6p	6
Ac12p	12

Nitrogen (99.999%) was the gas used for precursor atomization and plasma generation at 1.5 slm and 80 slm, respectively. Plasma power was set at 360 W. Four plasma-polymerized treatments with different coating passes (1, 2, 6 and 12) and AcAc as precursor liquid were applied on PLA Petri dishes (Table I). With a scanning pattern, the jet moved over the surface of PLA Petri dishes at a speed of 100 mm/min, a track pitch of 2 mm and a gap of 10 mm between the plasma gun and the PLA Petri dishes. Each analysis was performed in quadruplicate.

2.4. Morphological and chemical characterization

Roughness and surface topography of PLA Petri dishes were analyzed using a Multimode AFM Bruker instrument (Bruker Corporation, USA) with Nanoscope V Controller. The scanned area was 40 μm × 40 μm with a frequency of 50 Hz. NanoScope Analysis 1.4 (Bruker Corporation, USA) software was used in order to determine the morphological parameters: mean surface roughness (Ra) and developed interfacial area ratio (Sdr). Sdr parameter was calculated relating the real surface area and the projected area; and it was expressed as the percentage of additional surface area contributed by the texture compared to the scanned area [36]. Three areas per sample were studied, so that values corresponded to the average ones. Scanning Electron Microscope (SEM) HITACHI S-2400 with 18 kV power was employed to

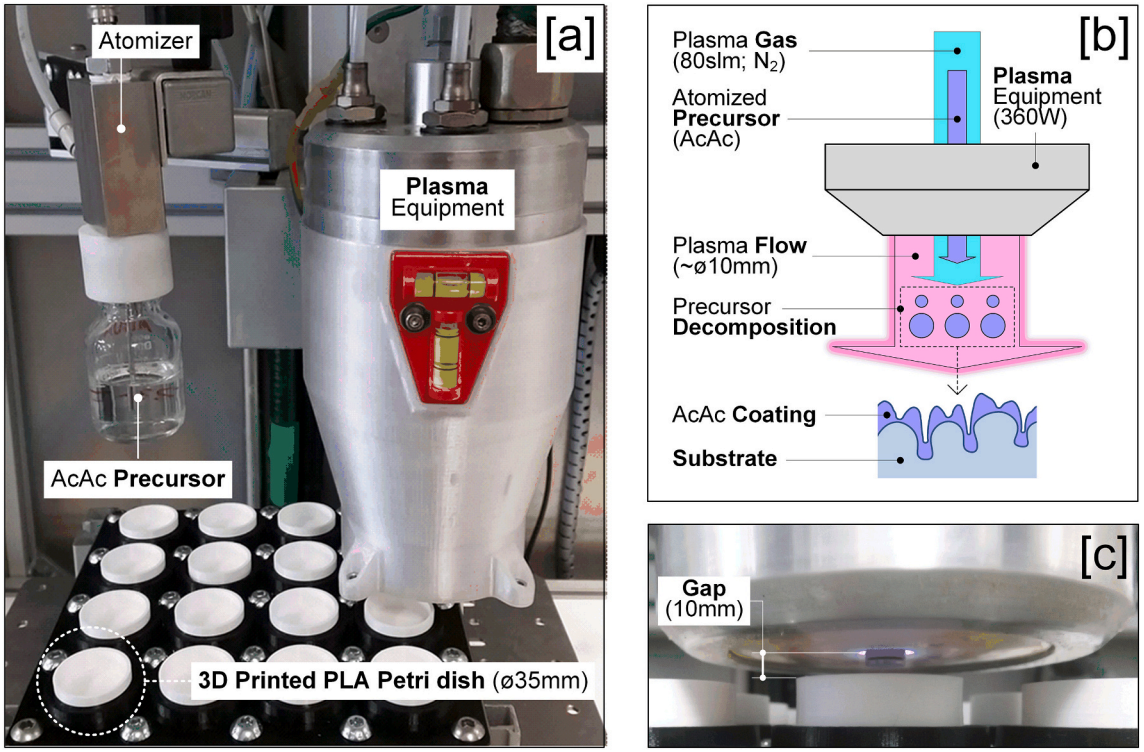

Fig. 1. Process sequence: [a] 3D printed PLA Petri dishes, [b] Close view of the deposition process, [c] Plasma-polymerization (APPJ) equipment and [d] Scheme of the plasma-polymerization process.

analyze the surface morphology of PLA Petri dishes, that were previously coated with gold and palladium to made them conductive.

The surface profiles of the dishes were studied from the AFM images. The signal distortion was firstly attenuated by image smoothing to avoid the detection of false peaks. Then, a threshold was applied to the peak amplitude to detect the true peaks and to neglect too small peaks. Finally, the positions of the identified peaks were determined and the distance between them was averaged.

The XPS analysis was used in order to obtain the chemical characterization of the coatings. X-ray photoelectron spectra were determined employing a Kratos AXIS Supra system (Kratos Analytical, England) with an hemispherical electrons analyzer and a Monochromatic AlKα X-ray source (120 W, 15 kV) operating at 1.33×10^{-7} Pa of residual pressure. Spectra were collected at 160 eV (general spectrums) and 20 eV (high resolution spectrums). Binding energies were related to C1s signal for the adventitious carbon at 285 eV. These results were deconvoluted by means of *PeakFit 4.12 (SPSS Inc.)*. Each sample was examined in triplicate.

2.5. Bacterial strains and growth conditions

The antimicrobial susceptible control *P. aeruginosa* PAO1 and *S. aureus* ATCC29213 strains, as well as the multidrug-resistant clinical *P. aeruginosa* Ps204, Ps713 and Ps1056, and meticillin-resistant clinical *S. aureus* W1569, W1570 and W1571 strains from the Molecular Microbiology Area collection (CIBIR, Spain) were included in all the experiments to perform the biofilm analysis. The strains were routinely grown onto Brain-Heart Infusion (BHI) agar (Pronadisa, Conda, Spain) at 37 °C during 18 h for culture and correct isolation of the colonies.

2.6. Biofilm quantification and bacterial growth

The total biofilm biomass production of the strains was analyzed by the CV staining protocol [37]. Briefly, an initial 10^6 CFU/mL bacterial inoculum prepared in 3 mL of Mueller Hinton (MH) Broth (Pronadisa, Conda, Spain) was inoculated on the PLA Petri dishes, and subsequently incubated at 37 °C during 24 h to obtain a mature biofilm. The medium was removed at the end of the incubation period, and the biofilm was washed with phosphate buffer saline (PBS) and fixed with methanol during 15 min at room temperature. Plates were dried during 10 min at room temperature after removing the methanol. Then, 3 mL of CV solution was added (Sigma, final concentration 10% in PBS) and incubated at room temperature during 20 min. The CV excess was removed under running water and dried. Finally, the cell bound crystal violet was dissolved in 3 mL of acetic acid 66% v/v, incubated at room temperature for 1 h and quantified by absorbance at 590 nm. Measures were performed on a plate reader (POLAR star Omega microplate reader, BMG Labtech). Three PLA Petri dishes with no treatment were included as control in all assays. Four PLA Petri dishes were used per each treatment and microorganism. ANOVA test has been realized to determine if there are statistically significant differences on biofilm formation between coated and untreated PLA Petri dishes.

3. Results and discussion

3.1. Chemical characterization

After applying the different plasma-polymerized coatings on the 3D printed PLA Petri dishes, the chemical modifications caused on the plates were evaluated by an XPS analysis. Fig. 2 illustrates the atomic chemical composition of untreated and coated PLA plates. Table II shows the relative abundances of the groups found in the deconvolution of the C1s high resolution spectra and the binding energies associated with their respective peaks.

The atomic composition of the untreated 3D printed PLA plate was: 71.80 ± 1.44% of C1s, 27.88 ± 1.46% of O1s and 0.06 ± 0.10% of N1s. This chemical composition was similar to that previously identified by Zhao et al. [38]. The percentage of carbon measured at the untreated 3D printed PLA was probably due to the presence of adventitious carbon on the plate surface. The carbon percentages of the different coated plates were due to both adventitious carbon and the provided one by the AcAc atomization. Higher superficial oxidation degree occurred in the coated plate than in the untreated plate (Fig. 2). This increase in the superficial oxygen percentage was significant since the first AcAc pass was applied, and it remained constant regardless of the number of plasma-polymerization passes. Nitrogen amount, were practically nonexistent (< 1%) for all samples. Three peaks were obtained in C1s spectra deconvolution (Table II): C-C/C-H at 285 eV, C—O at 286.5–287.2 eV and O-C=O at 288.5–289.3 eV [27,39,40]. Similar to above mentioned, oxygen functional groups (C—O, O-C=O) increased and carbon functional groups (C-C/C-H) decreased for Ac1p coatings. The increase in the superficial oxidation degree (O/C ratio), and specifically in carbonyl groups (O-C=O), could increase the surface free energy, thereby making the surface more hydrophilic [23,40].

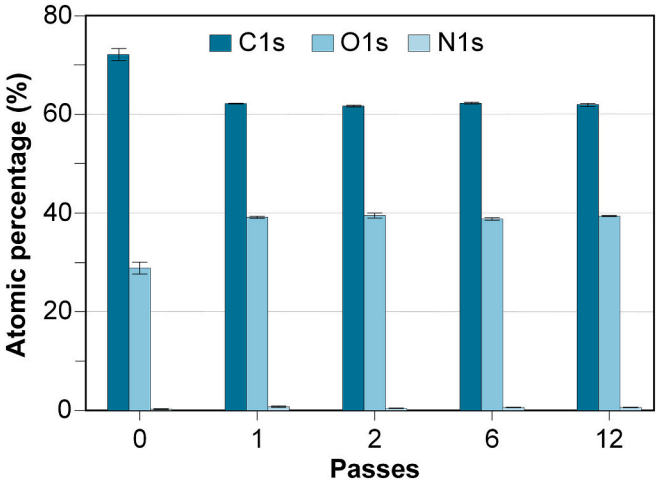

Fig. 2. Atomic percentages of C, O, N and Si of all the analyzed samples.

Table II
Relative percentages of groups found in the C1s signal of the analyzed samples.

Samples	C-C/C-H (~285 eV)	C-O (286.5–287.2 eV)	O-C=O (288.5–289.3 eV)
Untreated	57.64 ± 2.76	22.68 ± 0.83	19.68 ± 1.52
Ac1p	37.22 ± 0.29	31.41 ± 0.28	31.37 ± 0.09
Ac2p	37.60 ± 0.30	31.19 ± 0.14	31.21 ± 0.19
Ac6p	36.77 ± 0.08	31.41 ± 0.15	31.82 ± 0.14
Ac12p	36.83 ± 0.16	31.09 ± 0.32	32.08 ± 0.33

3.2. Morphological characterization

Fig. 3 illustrates SEM and AFM images of the untreated 3D printed PLA plates. The characteristic superficial pattern of FFF printing, with grooves due to the deposition of fused filament, is showed (Fig. 3[c]). The impossibility of setting up a water drop on those grooves involved that the wettability (water contact angle, WCA) of the plate surfaces was not measured. The SEM images magnification, increasing from x100 to x2000, provided a more detailed view of the PLA surface. The lumpy surface shows many spaces and holes where bacteria could attach and proliferate (Fig. 3[b,d]).

Fig. 4 shows SEM and AFM images of all the coated 3D printed PLA plates and Fig. 5 illustrates the mean surface roughness (Ra) and the developed interfacial area ratio (Sdr) of all samples. The so called “shadowing effect” occurred during deposition of plasma coatings. Plasma-polymerized particles could easily approach and deposit on

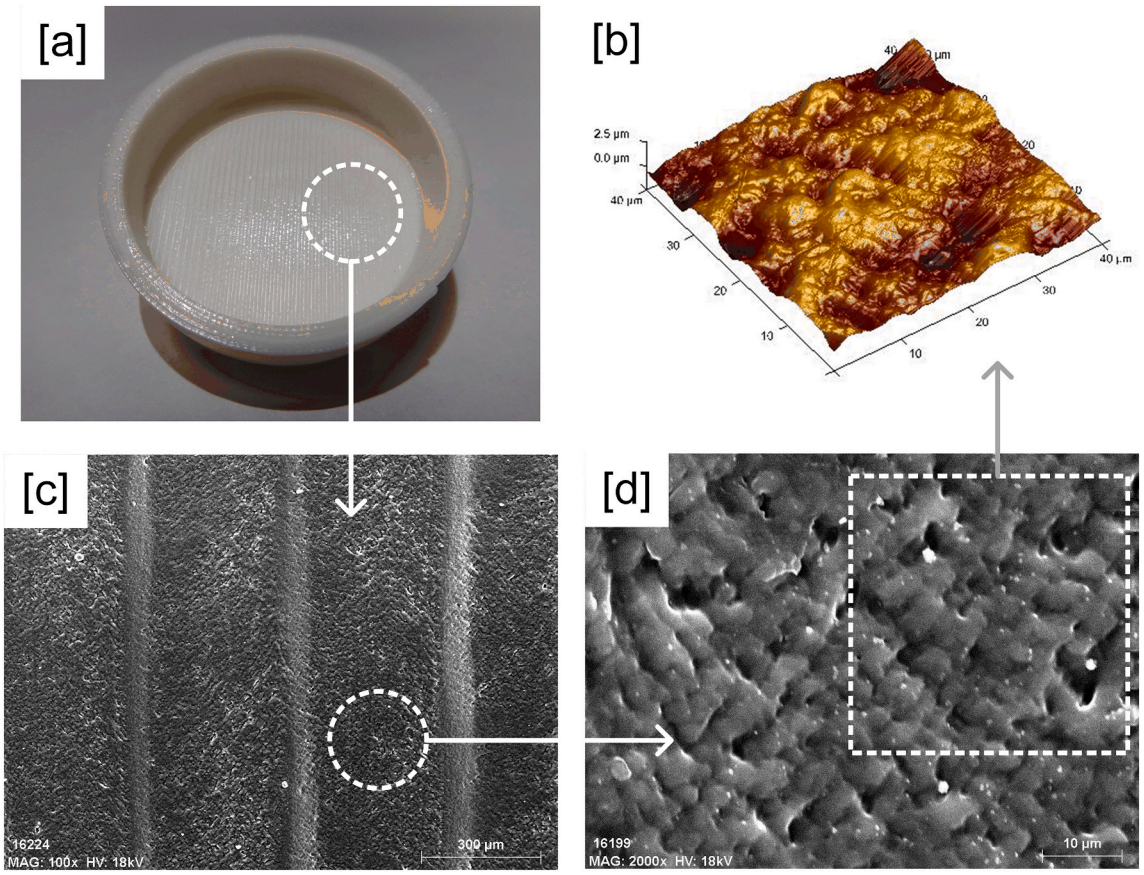

Fig. 3. Morphological characterization of the Untreated plate: [a] 3D printed PLA Petri dish, [b] AFM image (40x40µm), [c] SEM image (x100) and [d] SEM image (x2000).

higher surface points (hills). Then, these particles could either stick to such points or bounce off. Nonsticking particles were re-emitted and could arrive at lower surface points (valleys). This phenomenon leads to the generation of rougher surfaces [41].

During the first two passes (Fig. 4[a,b]), some of the plasma-polymerized particles were deposited on the higher points of the PLA surface whereas other particles were embedded into the lower points of the PLA surface, filling the surface grooves. This double effect caused an increment in the surface roughness and in the surface texture (Fig. 5). The most complex and textured surface was obtained when one AcAc pass was applied (Sdr: 8.6 ± 1.61%, Fig. 5). As a greater number of passes were applied, the AcAc coating was filling the surface grooves, so the surface irregularities decreased (Sdr: 2.62 ± 0.09%, Fig. 5). However, the highest surface roughness was obtained when two passes were applied (Ra: 531.5 ± 31.58 nm, Fig. 5). Most spaces were filled and disappeared after applying 6 passes (Fig. 4[c,d]), which led to a smoother surface and a lower roughness. When the greatest number of passes was applied (Ac12p), the plate surface showed lower roughness values than the untreated plates (Ra: 385.5 ± 9.40 nm, Fig. 5).

Fig. 6 shows the AFM profiles and distance between peaks of the

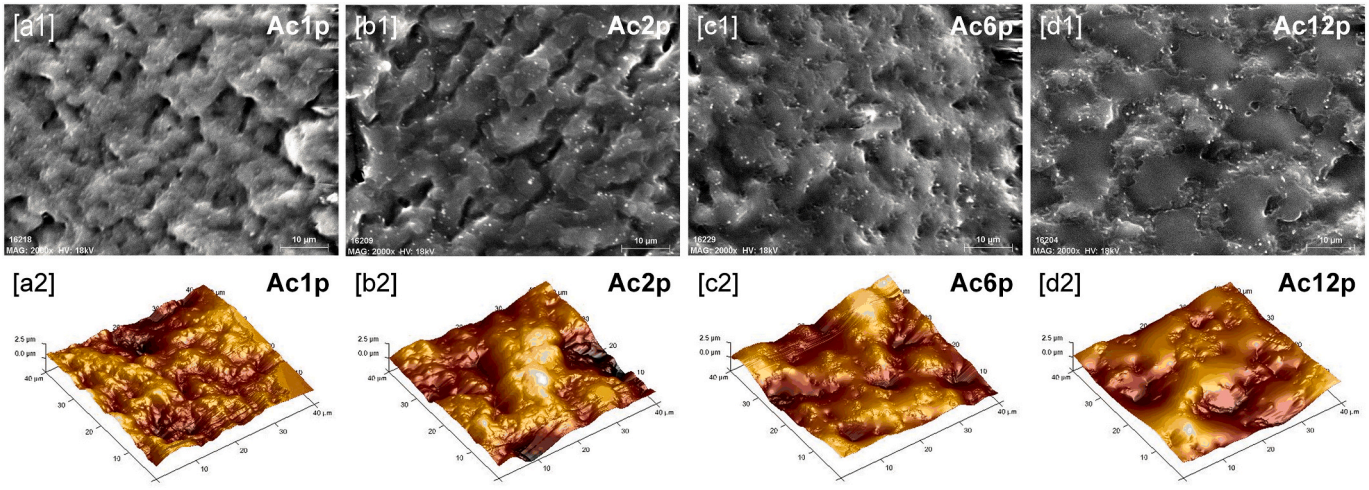

Fig. 4. AcAc coated plates: [1] SEM images (x2000) and [2] AFM images (40x40µm).

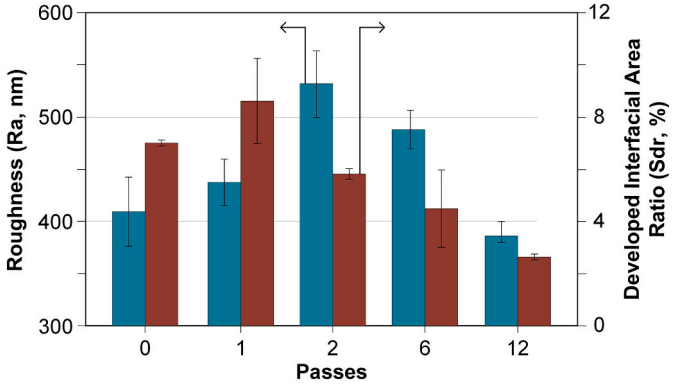

Fig. 5. Average roughness (Ra, nm) and developed interfacial area ratio (Sdr, %) of untreated and AcAc coated plates.

untreated and coated 3D printed PLA plates with one and two plasma passes. The distance between peaks of all analyzed samples is illustrated in Table III and these values agree with the degree of surface texturing (Sdr, Fig. 5). AFM profiles (Fig. 6[a2–c2]) confirmed the previously discussed deposition mechanism. Besides, it is possible to observe how the superficial pattern of untreated plates changed as the number of plasma passes increased. The distance between peaks decreased from 3.72 ± 1.89 μm (untreated plate) to 1.22 ± 0.84 μm and to 1.70 ± 1.22 μm with one (Ac1p) and two passes (Ac2p), respectively (Fig. 6[a3,b3]), but increased when higher numbers of passes were applied, that is to 6.67 ± 3.05 μm and 8.83 ± 3.67 μm for Ac6p and Ac12p, respectively (Table III). Fig. 6[a3–c3] shows how the coating formation process takes place as the successive plasma passes are applied. Fig. 6[b3] is configured from Fig. 6[a2] AFM profile, the deposited AcAc plasma-polymerized layer and the distance between peaks (which are obtained from Fig. 6[b2] AFM profile). On the other hand, Fig. 6[c3] is configured from Fig. 6[b3], adding one more AcAc pass and taking into account the distance between peaks (obtained from Fig. 6[c2]).

Thus, contrary to chemical characterization, the morphology of the coatings underwent changes that were influenced by the number of plasma-polymerization passes.

3.3. Biofilm quantification

As Fig. 7 illustrates, the relative biofilm percentages calculated by comparing the total biofilm biomass produced for each analyzed bacterial strain on coated versus untreated samples (control). The relative biofilm production for each strain on the untreated PLA dishes has been used as a reference (100%). Therefore, the coatings with relative biofilm productions higher than 100% were considered as probiofilm whereas those with relative biofilm productions lower than 100% were considered as antibiofilm.

A relationship between the number of plasma-polymerization passes and the biofilm production was characterized. The antibiofilm properties were obtained for all of the coatings with one pass, two passes (except for *S. aureus* ATCC29213) and six passes were deposited. Generally, the antibiofilm capacity increased as the number of passes decreased. Significant statistical differences ($p < 0.05$) were observed between the coatings applied with one, two and six passes regarding the untreated PLA plates; in terms of biofilm formation by all *P. aeruginosa* strains (except for *P. aeruginosa* Ps1056). The best antibiofilm capacity in *P. aeruginosa* strains was obtained with the coating Ac1p, that showed a relative biofilm production of 25.75 ± 3.73% for *P. aeruginosa* Ps204, 27.71 ± 3.53% for *P. aeruginosa* Ps713, 47.68 ± 9.48% for *P. aeruginosa* PAO1 and 85.30 ± 19.35% for *P. aeruginosa* Ps1056. Significant statistical differences ($p < 0.05$) in biofilm production were found for all *S. aureus* strains (with the exception of *S. aureus* ATCC29213 on Ac2p samples) when applying one, two and six passes in relation to untreated PLA plates. Regarding *S. aureus* strains, the best antibiofilm capacity (except for *S. aureus* ATCC29213) was achieved with the coating Ac2p. The relative biofilm production on Ac2p coatings was 40.14 ± 11.62% for *S. aureus* W1570, 40.93 ± 11.87% for *S. aureus* W1571, 47.96 ± 14.03% for *S. aureus* W1569 and 102.62 ± 13.37% for *S. aureus* ATCC29213.

We hypothesize that these results of biofilm production can be explained by the chemical and morphological characterizations of the samples.

XPS result showed that the chemical nature of the film generated is kept regardless of the number of passes applied and all the coatings produced carboxyl groups. These chemical bonds generate the hydration layer, which promote the antibiofilm capacity. The morphology of the coatings applied, expressed in terms of average roughness (Ra), developed interfacial area ratio (Sdr) and distance between peaks, is determined by the substrate morphology. In this study, we employed a rough surface (characteristic of FDM 3D printed objects). So, we need to deposit more than 6 passes of AcAc plasma-polymerized for filling the initial surface holes and consequently decrease the roughness values.

The chemical characterization results, described under Section 3.1, show an increment in oxygen-containing polar groups (C—O and O-C=O) when an AcAc coating is applied on 3D printed PLA plates. As previously reported [27,42], O-C=O groups are related with carboxylic groups and they are distinguished by their highly hydrophilic character. For that reason, plasma-polymerized coatings with high density of carboxylic groups can improve the hydrophilicity of the substrate.

The relationship between bacterial attachment and hydrophilic surfaces has been previously studied. Attractive interactions between the molecules and the surfaces give place when a hydrophilic surface is plunged in a fluid, which causes the water molecules to orientate towards the surface and generate a hydration layer. This layer causes a repulsive force on the surface resulting in a decrease in the bacterial adhesion (first step of biofilm production) [43].

Considering that all coatings tested in the present work showed the same surface chemistry regardless of the number of plasma-polymerization passes (Table II and Fig. 2), the differences in their antibiofilm capacity must be explained by other factors, such as the influence of the morphological changes produced.

According to Wenzel's model [44], a solid substrate with a positive wetting tendency will wet the more readily, the rougher its surface. On the other hand, if the smooth surface is water-repelling, the roughened surface will be more strongly so. More recently, other authors have obtained similar results in accordance with Wenzel's model. Jiang et al. [45], generated gel films with different surface roughness over glasses and silicon slices with the aim of studying the bacterial adhesion. They observed the magnification effect of surface roughness in the hierarchical structures. The water contact angle greatly decreased when increasing surface roughness if the surface was originally hydrophilic. This increase in the hydrophilic character reduced the bacterial adhesion, which was attributed to the formation of a tightly bound water layer adjacent to the film interface that brought repulsive forces between the bacteria and the gel films. Yuan et al. [46], applied an air plasma treatment over smooth and fibrous polystyrene (PS) films. They concluded that the surface roughness attributed to fibrous topography can amplify the intrinsic wettability or antiwettability.

Likewise, a relationship between the biofilm production (Fig. 7) and the roughness of the plates (Fig. 5) has been identified in this study. Generally, the higher roughness values and the better antibiofilm capacities (except for *S. aureus* ATCC29213) were obtained as the number of passes decreased from 12 to 2. When the number of passes decreased from 2 to 1, the surface roughness was reduced, and the biofilm productions of *P. aeruginosa* strains generally decreased whereas those of *S. aureus* strains generally increased.

With the aim of clarifying these aspects, Fig. 8 shows a scheme of the possible interaction of bacteria with the untreated and AcAc coated

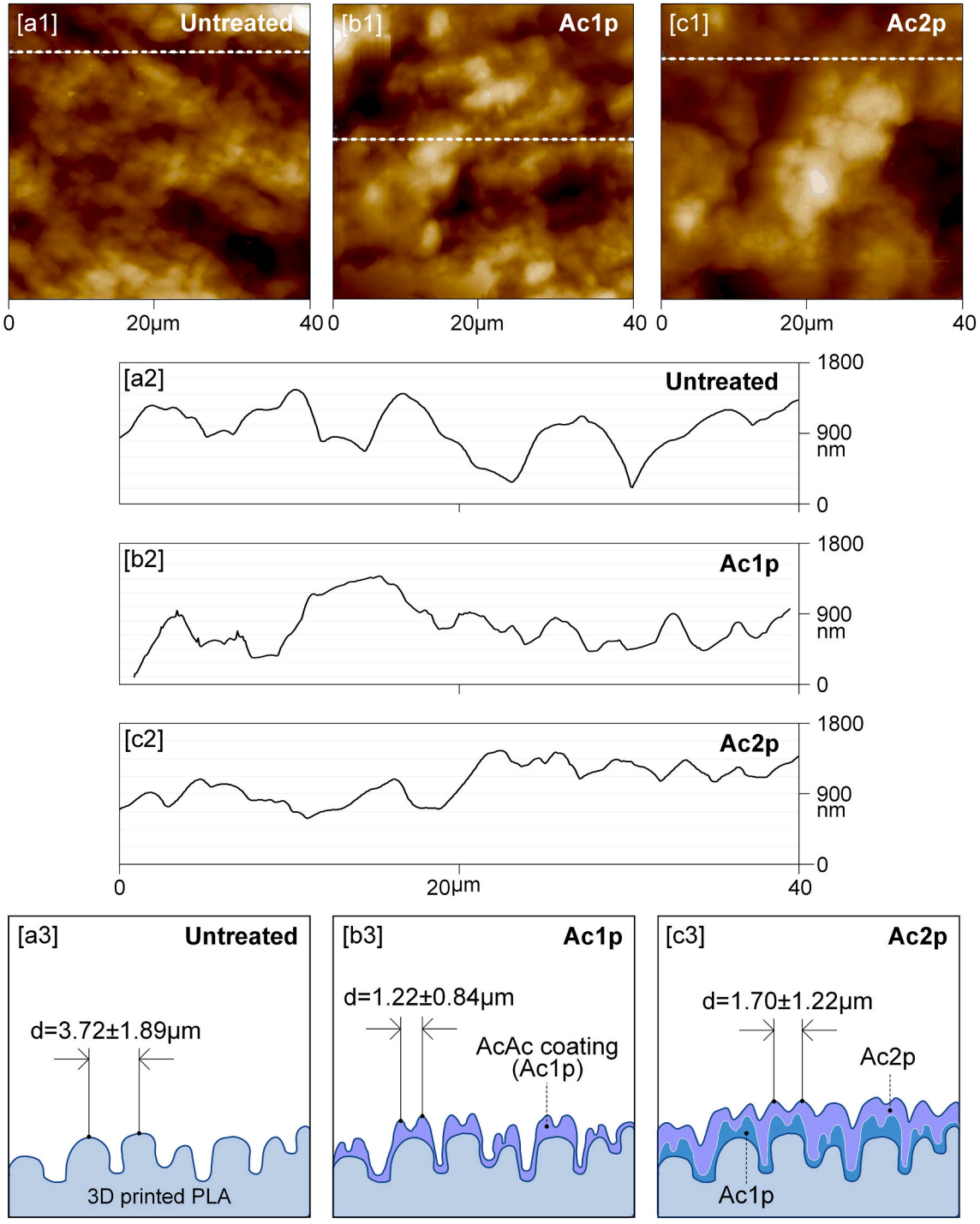

Fig. 6. Profiles of untreated and AcAc coated plates: [a] 2D-AFM images, [b] Cross section along the white dashed line and [c] Scheme of the coating deposition mechanism (d = distance between peaks, μm).

Table III
Distance between peaks of the analyzed samples.

Samples	Distance between peaks (μm)
Untreated	3.72 ± 1.89
Ac1p	1.22 ± 0.84
Ac2p	1.70 ± 1.22
Ac6p	6.67 ± 3.05
Ac12p	8.83 ± 3.67

plates according to the surface roughness and the thickness of the hydration layer. As the chemical characterization suggested, the plasma-polymerized coatings may have increased the hydrophilic character of the samples by providing their surface chemistry with polar groups, which would promote surface hydration and consequently, a repulsive force (Fig. 8[a,c]). In addition, the reduction of the number of plasma-polymerization passes caused an increase in the surface roughness. Such roughening effect could magnify the hydrophilicity of the coatings and hence, the repulsive forces that would hinder bacterial adhesion (Fig. 8[c–f]). This seems evident for the interaction of the coatings with *S. aureus* strains, which showed the highest and lowest biofilm

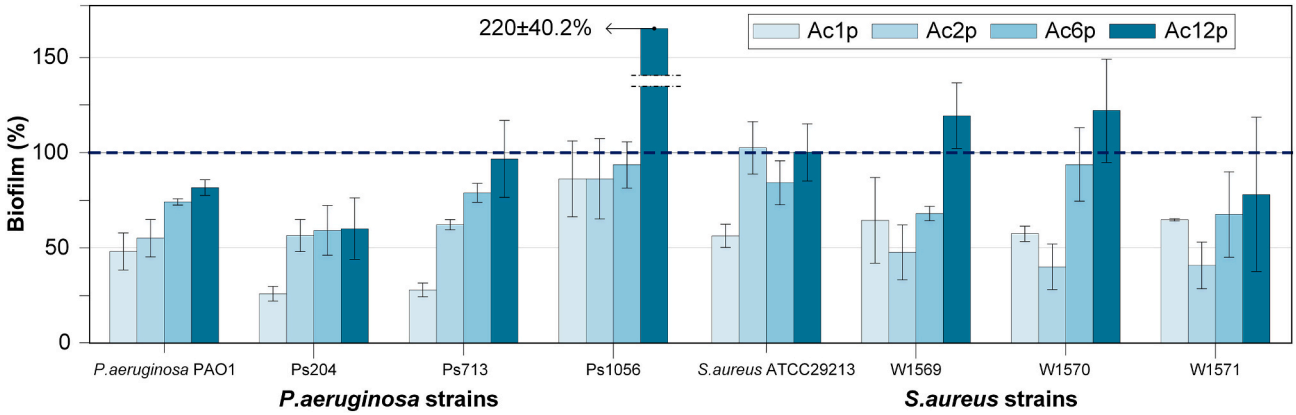

Fig. 7. Relative biofilm production generated on coated 3D printed PLA plates by *P. aeruginosa* and *S. aureus* strains. The blue dashed line indicates the biofilm production for each strain on untreated 3D printed PLA plates (100%). (For interpretation of the references to color in this figure legend, the reader is referred to the web version of this article.)

productions on the coatings with the lowest and the highest roughness values, respectively (with the exception of *S. aureus* ATCC29213).

The different behavior of *P. aeruginosa* strains on sample Ac1p can be explained by the size and shape of these bacteria and the profiles of the plates [47]. As other authors have defined, the rough patterns are propitious to reduce bacterial attachment and, consequently, biofilm production. In contrast, the biofilm formation is favored by smooth surfaces, where the bacteria tend to accumulate in large groups. In particular, when the distance between peaks is lower than the bacterial size, they undergo structural modifications that hinder the superficial adhesion [48]. They might even cause an elongation of the cell membrane, its subsequent rupture and, consequently, the cell death [49]. *P. aeruginosa* is a Gram-negative and rod-shaped (0.5–1 μm width and 2–4 μm length) bacterium, while *S. aureus* is a Gram-positive and round-shaped (0.5–1 μm diameter) bacterium [48]. Ac1p is the coating which presents the lowest distance between peaks and the maximum Sdr value (1.22 ± 0.84 μm and 8.6 ± 1.61%, respectively). These spaces between peaks are 2–3 times lower than *P. aeruginosa* length (Fig. 8[b]) and could reduce their adhesion for any of the aforementioned reasons. For these reasons, Ac1p coating resulted in the lowest biofilm production by *P. aeruginosa* strains. On the other hand, the length of *S. aureus* bacteria (Fig. 8[c–f]) is lower than the space between peaks of any of the AcAc coatings in the present study. So, for these strains, the distance between peaks had no effect on the biofilm production.

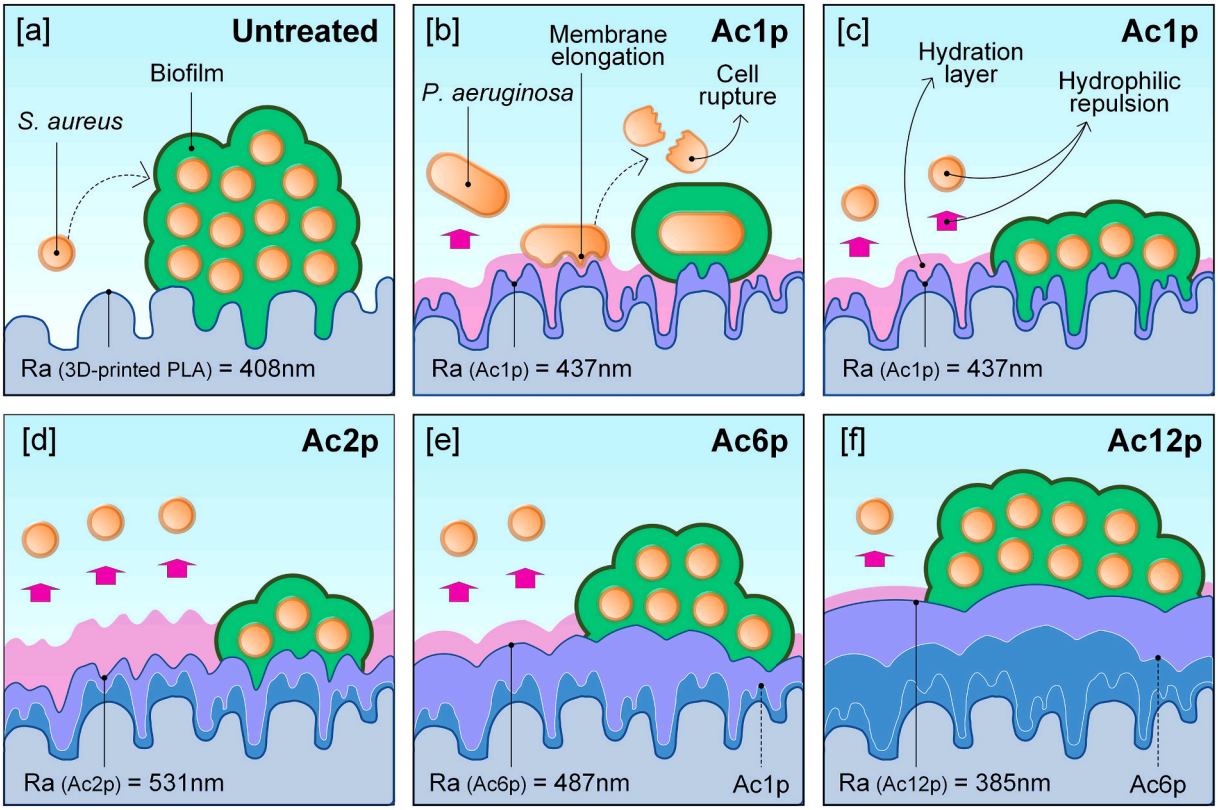

Fig. 8. Scheme of bacterial behavior according to the surface morphology and the consequent hydration layer generated: [a] Untreated, [b] *P. aeruginosa* interaction on Ac1p, and *S. aureus* interaction on [c] Ac1p, [d] Ac2p, [e] Ac6p and [f] Ac12p.

4. Conclusions

In this research, AcAc coatings with different numbers of passes were deposited by plasma-polymerization on the surface of 3D printed PLA Petri dishes with the objective of reducing the biofilm production of multidrug-resistant and susceptible *P. aeruginosa* and *S. aureus* strains. It has been verified that atmospheric pressure plasma technology is useful for this purpose and an innovative solution for employing 3D printed objects in the clinical field (nowadays, in constant growing). The disinfectant liquids could damage the printed objects and significantly reduce the number of uses. And although large reductions in biofilm formation have not been obtained, the plasma-polymerized coatings developed in this study, can reduce the bacteria attachment and biofilm production and disinfectant solutions concentration; increasing the lifetime of 3D printed elements in facial mask.

The key findings of this study are the following:

- All AcAc coatings applied with 1, 2 or 6 passes, except Ac2p in *S. aureus* ATCC29213, showed an antibiofilm capacity for all bacteria analyzed.
- The smaller the number of applied passes, the better the antibiofilm properties of the coatings. The best antibiofilm coatings for *P. aeruginosa* and *S. aureus* strains were Ac1p and Ac2p, respectively; which reduced biofilm formation more than 50% regarding the untreated PLA Petri dishes.
- AcAc plasma-polymerized coatings caused an increment of oxygen polar groups (C—O and O-C=O) on 3D printed PLA substrates. This increment could produce a hydrophilic character of the coatings. Regardless of the number of passes applied, no variation in the chemical composition of the coatings was observed. Therefore, the biofilm reductions could be caused by a combined effect of the new chemical and morphological surface properties.
- According to Wenzel's model, hydrophilic surfaces will become even more hydrophilic as their roughness increases. For this reason, the antibiofilm capacity of the coatings studied in the present work was generally greater as the coating surfaces became rougher. This was more evident for the *S. aureus* strains, with most of them showing their lowest biofilm productions on the roughest coating (Ac2p). For *P. aeruginosa* strains, the Ac1p coating produced greater antibiofilm capacity than Ac2p coating. This fact may be due to the surface texture modifications produced by Ac1p coating, which reduced 2–3 times the distance between peaks regarding the bacterial cellular length, leading to a reduced contact area between the bacteria and the coating, as well as to the potential rupture of the cellular membrane.

CRediT authorship contribution statement

Ignacio Muro-Fraguas: Conceptualization, Methodology, Validation, Formal analysis, Investigation, Data curation, Writing - original draft, Visualization. **Ana Sainz-García**: Conceptualization, Methodology, Validation, Formal analysis, Investigation, Data curation, Writing - review & editing, Visualization. **María López**: Conceptualization, Methodology, Validation, Formal analysis, Investigation, Data curation, Writing - review & editing. **Beatriz Rojo-Bezares**: Conceptualization, Methodology, Validation, Formal analysis, Investigation, Data curation, Writing - review & editing. **Rodolfo Múgica-Vidal**: Conceptualization, Methodology, Formal analysis, Investigation, Data curation, Writing - review & editing, Visualization. **Elisa Sainz-García**: Conceptualization, Methodology, Formal analysis, Investigation, Data curation, Writing - review & editing, Visualization. **Paula Toledano**: Conceptualization, Methodology, Validation, Formal analysis, Investigation, Data curation, Writing - review & editing. **Yolanda Sáenz**: Conceptualization, Methodology, Validation, Formal analysis, Investigation, Resources, Data curation, Writing - review & editing, Supervision, Project administration. **Ana González-Marcos**: Conceptualization, Methodology, Software, Formal analysis, Investigation, Resources, Data curation, Writing - review & editing, Visualization, Supervision, Project administration. **Fernando Alba-Elías**: Conceptualization, Methodology, Formal analysis, Investigation, Resources, Data curation, Writing - review & editing, Visualization, Supervision, Project administration, Funding acquisition.

Declaration of competing interest

The authors declare that they have no known competing financial interests or personal relationships that could have appeared to influence the work reported in this paper.

Acknowledgements

This work was supported by the Ministerio de Economía, Industria y Competitividad of Spain (MINECO) (project AGL2017-82779-C2-R "Programa Estatal de I+D+i Orientada a los Retos de la Sociedad") and co-funded by European Regional Development Fund (FEDER) "A way to make Europe". XPS tests were conducted by the Advanced Microscopy Laboratory (LMA) of The Institute of Nanosciences of Aragon (INA), University of Zaragoza. The authors are thankful to the LMA-INA for the access to their equipment and their expertise. The AFM images were taken by the Central Research Support Service (SCAI) of the University of Málaga (UMA). The author E. Sainz-García, as postdoctoral researcher of the University of La Rioja, thanks the postdoctoral training program that is funded by the Plan Propio of the University of La Rioja. The author I. Muro-Fraguas, thanks the program of pre-doctoral contracts for the training of research staff funded by the University of La Rioja.

References

[1] A. Unkovskiy, P.H.B. Bui, C. Schille, J. Geis-Gerstorfer, F. Huettig, S. Spintzyk, Objects build orientation, positioning, and curing influence dimensional accuracy and flexural properties of stereolithographically printed resin, Dent. Mater. 34 (2018) e324–e333, https://doi.org/10.1016/j.dental.2018.09.011.
[2] Wohlers Associates, Wohlers report 2017 service provider survey results, https://www.i3dmfg.com/wp-content/uploads/2017/07/Wohlers-Report-2017-Service-Provider-Survey-Results.pdf, (2017) , Accessed date: 2 May 2019.
[3] J. Domínguez-Robles, N. Martin, M. Fong, S. Stewart, N. Irwin, M. Rial-Hermida, R. Donnelly, E. Larrañeta, J. Domínguez-Robles, N.K. Martin, M.L. Fong, S.A. Stewart, N.J. Irwin, M.I. Rial-Hermida, R.F. Donnelly, E. Larrañeta, Antioxidant PLA composites containing lignin for 3D printing applications: a potential material for healthcare applications, Pharmaceutics 11 (2019) 165, https://doi.org/10.3390/pharmaceutics11040165.
[4] C. Lee Ventola, Medical applications for 3D printing: current and projected uses, P T 39 (2014) 704–711.
[5] Q. Yan, H. Dong, J. Su, J. Han, B. Song, Q. Wei, Y. Shi, A review of 3D printing technology for medical applications, Engineering 4 (2018) 729–742, https://doi.org/10.1016/j.eng.2018.07.021.
[6] E. Commission, Conformity Assessment Procedures for 3D Printing and 3D Printed Products to be used in a Medical Context for COVID-19, (2020), pp. 4–7 https://ec.europa.eu/docsroom/documents/40562.
[7] J.P. Sallés, Design of a 3D printed surgical guide to assist bone graft surgical interventions, Bacherlor´s degree final project, University of Pompeu Fabra, Barcelona, Spain, 2017.
[8] G. Valero, Surface finishing guidebook, Met. Finish. Mag. 109 (2011).
[9] W.G. Ragland III, R. Prototyping Center, S. Kumpaty, S. Kamara, N. Kanoongo, G. Raju, N. Phule, N. Panda, K. Balasubramanian, Surface finish analysis of surgical tools created by direct metal laser sintering and subtractive manufacturing, https://www.ncurproceedings.org/ojs/index.php/NCUR2012/article/view/48, (2012) , Accessed date: 27 June 2020.
[10] J. Lipton, J. Witzleben, V. Green, C. Ryan, H. Lipson, Demonstrations of additive manufacturing for the hospitality industry, 3D Print. Addit. Manuf. 2 (2015) 204–208, https://doi.org/10.1089/3dp.2015.0031.
[11] T.M. Rankin, N.A. Giovinco, D.J. Cucher, G. Watts, B. Hurwitz, D.G. Armstrong, Three-dimensional printing surgical instruments: are we there yet? J. Surg. Res. 189 (2014) 193–197, https://doi.org/10.1016/j.jss.2014.02.020.
[12] M. Wang, T. Tang, Surface treatment strategies to combat implant-related infection from the beginning, J. Orthop. Transl. 17 (2019) 42–54, https://doi.org/10.1016/j.jot.2018.09.001.
[13] K.S. Aiyer, B.S. Vijayakumar, A.S. Vishwanathan, The enigma of biofilms, Curr. Sci.

115 (2018) 204–205, https://doi.org/10.18520/cs/v115/i2/204-205.
[14] D. Popescu, D. Anania, C. Amza, D. Cicic, Design and rapid manufacturing of patient-specific spinal surgical guides: a survey, Proc. Manuf. Syst. 7 (2012) 115–1.
[15] R. Pérez-Mañanes, J. Calvo-Haro, J. Arnal-Burró, F. Chana-Rodríguez, P. Sanz-Ruiz, J. Vaquero-Martín, Nuestra experiencia con impresión 3D doméstica en Cirugía Ortopédica y Traumatología. Hazlo tú mismo, Rev. Latinoam. Cirugía Ortopédica. 1 (2016) 47–53, https://doi.org/10.1016/j.rslaot.2016.06.004.
[16] D. Shilo, O. Emodi, O. Blanc, D. Noy, A. Rachmiel, Printing the future—updates in 3D printing for surgical applications, Rambam Maimonides Med. J. 9 (2018) e0020, , https://doi.org/10.5041/rmmj.10343.
[17] F. Alba-Elías, J. Ordieres-Meré, A. González-Marcos, Deposition of thin-films on EPDM substrate with a plasma-polymerized coating, Surf. Coatings Technol. 206 (2011) 234–242, https://doi.org/10.1016/J.SURFCOAT.2011.06.054.
[18] A. Anagri, A. Baitukha, C. Debiemme-Chouvy, I.T. Lucas, J. Pulpytel, T.T.M. Tran, S. Tabibian, F. Arefi-Khonsari, Nanocomposite coatings based on graphene and siloxane polymers deposited by atmospheric pressure plasma. Application to corrosion protection of steel, Surf. Coatings Technol. 377 (2019) 124928, , https://doi.org/10.1016/j.surfcoat.2019.124928.
[19] R. Múgica-Vidal, F. Alba-Elías, E. Sainz-García, J. Ordieres-Meré, Atmospheric plasma-polymerization of hydrophobic and wear-resistant coatings on glass substrates, Surf. Coatings Technol. 259 (2014) 374–385, https://doi.org/10.1016/j.surfcoat.2014.10.067.
[20] R. Múgica-Vidal, F. Alba-Elías, E. Sainz-García, A. González-Marcos, Reducing friction on glass substrates by atmospheric plasma-polymerization of APTES, Surf. Coatings Technol. 309 (2017) 1062–1071, https://doi.org/10.1016/j.surfcoat.2016.10.030.
[21] R. Davis, A. El-Shafei, P. Hauser, Use of atmospheric pressure plasma to confer durable water repellent functionality and antimicrobial functionality on cotton/polyester blend, Surf. Coatings Technol. 205 (2011) 4791–4797, https://doi.org/10.1016/j.surfcoat.2011.04.035.
[22] D. Duday, C. Vreuls, M. Moreno, G. Frache, N.D. Boscher, G. Zocchi, C. Archambeau, C. Van De Weerdt, J. Martial, P. Choquet, Atmospheric pressure plasma modified surfaces for immobilization of antimicrobial nisin peptides, Surf. Coatings Technol. 218 (2013) 152–161, https://doi.org/10.1016/j.surfcoat.2012.12.045.
[23] E. Baran, H. Erbil, E.H. Baran, H.Y. Erbil, Surface modification of 3D printed PLA objects by fused deposition modeling: a review, Colloids and Interfaces 3 (2019) 43, https://doi.org/10.3390/colloids3020043.
[24] C.P. Stallard, K.A. McDonnell, O.D. Onayemi, J.P. O'Gara, D.P. Dowling, Evaluation of protein adsorption on atmospheric plasma deposited coatings exhibiting superhydrophilic to superhydrophobic properties, Biointerphases. 7 (2012) 1–12, https://doi.org/10.1007/s13758-012-0031-0.
[25] M. Hernández-Orta, E. Pérez, L.E. Cruz-Barba, M.A. Sánchez-Castillo, Synthesis of bactericidal polymer coatings by sequential plasma-induced polymerization of 4-vinyl pyridine and gas-phase quaternization of poly-4-vinyl pyridine, J. Mater. Sci. 53 (2018) 8766–8785, https://doi.org/10.1007/s10853-018-2183-x.
[26] R. Múgica-Vidal, E. Sainz-García, A. Álvarez-Ordóñez, M. Prieto, M. González-Raurich, M. López, M. López, B. Rojo-Bezares, Y. Sáenz, F. Alba-Elías, Production of antibacterial coatings through atmospheric pressure plasma: a promising alternative for combatting biofilms in the food industry, Food Bioprocess Technol. (2019), https://doi.org/10.1007/s11947-019-02293-z.
[27] I. Muro-Fraguas, A. Sainz-García, P. Fernández Gómez, M. López, R. Múgica-Vidal, E. Sainz-García, P. Toledano, Y. Sáenz, M. López, M. González-Raurich, M. Prieto, A. Alvarez-Ordóñez, A. González-Marcos, F. Alba-Elías, Atmospheric pressure cold plasma anti-biofilm coatings for 3D printed food tools, Innov. Food Sci. Emerg. Technol. 64 (2020), https://doi.org/10.1016/j.ifset.2020.102404.
[28] K. Poole, Pseudomonas aeruginosa: resistance to the max, Front. Microbiol. 2 (2011), https://doi.org/10.3389/fmicb.2011.00065.
[29] S. Hogan, J.P. O'Gara, E. O'Neill, Novel treatment of staphylococcus aureus device-related infections using fibrinolytic agents, Antimicrob. Agents Chemother. 62 (2018), https://doi.org/10.1128/AAC.02008-17.
[30] S.S.P. Hsu, J. Gateno, R.B. Bell, D.L. Hirsch, M.R. Markiewicz, J.F. Teichgraeber, X. Zhou, J.J. Xia, Accuracy of a computer-aided surgical simulation protocol for orthognathic surgery: a prospective multicenter study, J. Oral Maxillofac. Surg. 71 (2013) 128–142, https://doi.org/10.1016/j.joms.2012.03.027.
[31] S. Mardini, S. Alsubaie, C. Cayci, H. Chim, N. Wetjen, Three-dimensional preoperative virtual planning and template use for surgical correction of craniosynostosis, J. Plast. Reconstr. Aesthetic Surg. 67 (2014) 336–343, https://doi.org/10.1016/j.bjps.2013.11.004.
[32] H. Herrero Antón de Vez, J. Herrero Jover, C. Silva-Vergara, Personalized 3d printed surgical tool for guiding the chisel during hump reduction in rhinoplasty, Plast. Reconstr. Surg. - Glob. Open. 6 (2018), https://doi.org/10.1097/GOX.0000000000001668.
[33] Y.L. Chuan, S.A.K. Pandya, Fabrication of non-implant 3D printed skin, MATEC Web Conf., EDP Sciences, 2018, https://doi.org/10.1051/matecconf/201815202016.
[34] G.R.J. Swennen, L. Pottel, P.E. Haers, Custom-made 3D-printed face masks in case of pandemic crisis situations with a lack of commercially available FFP2/3 masks, Int. J. Oral Maxillofac. Surg. 49 (2020) 673–677, https://doi.org/10.1016/j.ijom.2020.03.015.
[35] Product datasheet PLA, 25 (2020).
[36] A. Bonyár, AFM characterization of the shape of surface structures with localization factor, Micron 87 (2016) 1–9, https://doi.org/10.1016/j.micron.2016.05.002.
[37] E. Peeters, H.J. Nelis, T. Coenye, Comparison of multiple methods for quantification of microbial biofilms grown in microtiter plates, J. Microbiol. Methods 72 (2008) 157–165, https://doi.org/10.1016/j.mimet.2007.11.010.
[38] Y. Zhao, A. Fina, A. Venturello, F. Geobaldo, Effects of gas atmospheres on poly (lactic acid) film in acrylic acid plasma treatment, Appl. Surf. Sci. 283 (2013) 181–187, https://doi.org/10.1016/j.apsusc.2013.06.078.
[39] H. Abourayana, P. Dobbyn, D. Dowling, Enhancing the mechanical performance of additive manufactured polymer components using atmospheric plasma pre-treatments, Plasma Process. Polym. 15 (2018), https://doi.org/10.1002/ppap.201700141.
[40] M. Wang, P. Favi, X. Cheng, N.H. Golshan, K.S. Ziemer, M. Keidar, T.J. Webster, Cold atmospheric plasma (CAP) surface nanomodified 3D printed polylactic acid (PLA) scaffolds for bone regeneration, Acta Biomater. 46 (2016) 256–265, https://doi.org/10.1016/J.ACTBIO.2016.09.030.
[41] A. Ganvir, Microstructure and thermal conductivity of liquid feedstock plasma sprayed thermal barrier coatings, https://www.researchgate.net/publication/310403458_Microstructure_and_Thermal_Conductivity_of_Liquid_Feedstock_Plasma_Sprayed_Thermal_Barrier_Coatings, (2016) , Accessed date: 17 March 2020.
[42] M.C. Ramkumar, K. Navaneetha Pandiyaraj, A. Arun Kumar, P.V.A. Padmanabhan, P. Cools, N. De Geyter, R. Morent, S. Uday Kumar, V. Kumar, P. Gopinath, S.K. Jaganathan, R.R. Deshmukh, Atmospheric pressure non-thermal plasma assisted polymerization of poly (ethylene glycol) methylether methacrylate (PEGMA) on low density polyethylene (LDPE) films for enhancement of biocompatibility, Surf. Coatings Technol. 329 (2017) 55–67, https://doi.org/10.1016/j.surfcoat.2017.09.020.
[43] M. Temmen, O. Ochedowski, M. Schleberger, M. Reichling, T.R.J. Bollmann, Hydration layers trapped between graphene and a hydrophilic substrate, New J. Phys. 16 (2014), https://doi.org/10.1088/1367-2630/16/5/053039.
[44] R.N. Wenzel, Resistance of solid surfaces to wetting by water, Ind. Eng. Chem. 28 (1936) 988–994, https://doi.org/10.1021/ie50320a024.
[45] Y. Jiang, Y.J. Yin, X.C. Zha, X.Q. Dou, C.L. Feng, Wettability regulated gram-negative bacterial adhesion on biomimetic hierarchical structures, Chinese Chem. Lett. 28 (2017) 813–817, https://doi.org/10.1016/j.cclet.2016.08.002.
[46] Y. Yuan, M.P. Hays, P.R. Hardwidge, J. Kim, Surface characteristics influencing bacterial adhesion to polymeric substrates, RSC Adv. 7 (2017) 14254–14261, https://doi.org/10.1039/c7ra01571b.
[47] M. Kargar, Y.R. Chang, H. Khalili Hoseinabad, A. Pruden, W.A. Ducker, Colloidal crystals delay formation of early stage bacterial biofilms, ACS Biomater. Sci. Eng. 2 (2016) 1039–1048, https://doi.org/10.1021/acsbiomaterials.6b00163.
[48] S. Wu, S. Altenried, A. Zogg, F. Zuber, K. Maniura-Weber, Q. Ren, Role of the surface nanoscale roughness of stainless steel on bacterial adhesion and microcolony formation, ACS Omega 3 (2018) 6456–6464, https://doi.org/10.1021/acsomega.8b00769.
[49] A. Elbourne, R.J. Crawford, E.P. Ivanova, Nano-structured antimicrobial surfaces: from nature to synthetic analogues, J. Colloid Interface Sci. 508 (2017) 603–616, https://doi.org/10.1016/j.jcis.2017.07.021.